

Hierarchically porous $\text{TiO}_2@\text{C}$ membrane with oxygen vacancy: A novel platform for enhancing catalytic conversion of polysulfides

Sheng-You Qiu,^a Chuang Wang,^a Liang-Liang Gu,^a Ke-Xin Wang,^a Xiao-Tian Gao,^a Jian Gao,^b Zaixing Jiang,^{*a} Jian Gu,^{*c} Xiao-Dong Zhu^{*b,a}

^aSchool of Chemistry and Chemical Engineering, Harbin Institute of Technology, Harbin, 150001, China. E-mail: jiangzaixing@hit.edu.cn; zxd9863@163.com.

^bState Key Laboratory Base of Eco-Chemical Engineering, College of Chemical Engineering, Qingdao University of Science & Technology, Qingdao, 266042, China. E-mail: xiao-dong_zhu@qust.edu.cn.

^cScience and Technology on Aerospace Chemical Power Laboratory, Hubei Institute of Aerospace Chemotechnology, Xiangyang 441003, China. E-mail: gujian9804@163.com.

Computational method

The Vienna Ab Initio Package (VASP) have been employed to perform all the density functional theory (DFT) calculations within the generalized gradient approximation (GGA) using the PBE formulation.¹⁻³ The projected augmented wave (PAW) potentials have been chosen to describe the ionic cores and take valence electrons into account using a plane wave basis set with a kinetic energy cutoff of 450 eV.^{4,5} Partial occupancies of the Kohn-Sham orbitals were allowed using the Gaussian smearing method and a width of 0.05 eV. The on-site corrections (DFT+U) have been applied to the 3d electron of Ti atoms ($U_{\text{eff}}=4.5$ eV) by the approach from Dudarev et al.⁶ The electronic energy was considered self-consistent when the energy change was smaller than 10^{-5} eV. A geometry optimization was considered convergent when the force change was smaller than 0.02 eV/Å. Grimme's DFT-D3 methodology was used to describe the dispersion interactions.⁷

The equilibrium lattice constant of hexagonal graphene monolayer unit cell separated by a vacuum layer in the depth of 15 Å was optimized, when using a $15\times15\times15$ Monkhorst-Pack k-point grid for Brillouin zone sampling, to be $a=2.468$ Å. We then use it to construct a graphene monolayer model with $p(6\times6)$ periodicity in the x and y directions and 4 atomic layers in the z direction by vacuum depth of 15 Å in order to separate the surface slab from its periodic duplicates. This graphene model comprises of 72 C atoms. During structural optimizations, the gamma point in the Brillouin zone was used for k-point sampling, and all atoms were allowed to relax.

The equilibrium lattice constants of anatase TiO_2 unit cell were optimized, when using a $10\times10\times4$ Monkhorst-Pack k-point grid for Brillouin zone sampling, to be $a=b=3.858$ Å and $c=9.652$ Å. We then use it to construct an anatase- $\text{TiO}_2(101)$ surface model with $p(1\times3)$ periodicity in the x and y directions and 2 stoichiometric layers in the z direction by vacuum depth of 15 Å in order to separate the surface slab from its periodic duplicates. This anatase- $\text{TiO}_2(101)$ surface model contains 24 Ti and 48 O atoms. In another anatase- $\text{TiO}_2(101)$ surface model, one O atom on the outmost layer of the anatase- $\text{TiO}_2(101)$ surface model above was removed order to form an oxygen vacancy. During structural optimizations, the gamma point in the Brillouin zone was used for k-point sampling, and the top stoichiometric layer was allowed to fully relax while the bottom one was fixed.

The adsorption energy (E_{ads}) of adsorbate A was defined as $E_{\text{ads}}=E_{\text{A/surf}}-E_{\text{surf}}-E_{\text{A(g)}}$, where $E_{\text{A/surf}}$, E_{surf} and $E_{\text{A(g)}}$ are the energy of adsorbate A adsorbed on the surface, the energy of clean surface, and the energy of isolated A molecule in a cubic periodic box with a side length of 20 Å and a $1\times1\times1$ Monkhorst-Pack k-point grid for Brillouin zone sampling, respectively.

The free energy of a gas phase molecule or an adsorbate on the surface was calculated by the equation $G=E+ZPE-TS$, where E is the total energy, ZPE is the zero-point energy, T is the temperature in kelvin (298.15 K is set here), and S is the entropy.

Supplementary Figures

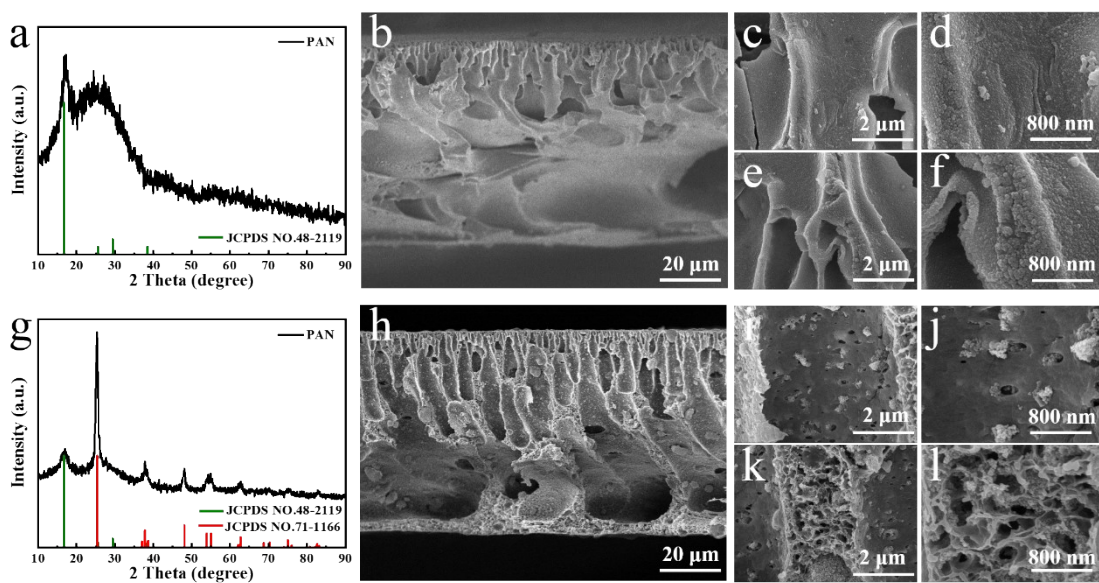


Figure S1 (a) XRD patterns of PAN membrane and corresponding PDF card; SEM images of (b) the cross section of PAN membrane, (c, d) the internal pore surface of PAN membrane, (e, f) the cross section of the pore wall of PAN membrane; (g) XRD patterns of TiO_2 @PAN membrane and corresponding PDF cards; SEM images of (h) the cross section of TiO_2 @PAN membrane, (i, j) the internal pore surface of TiO_2 @PAN membrane, (k, l) the cross section of the pore wall of TiO_2 @PAN membrane.

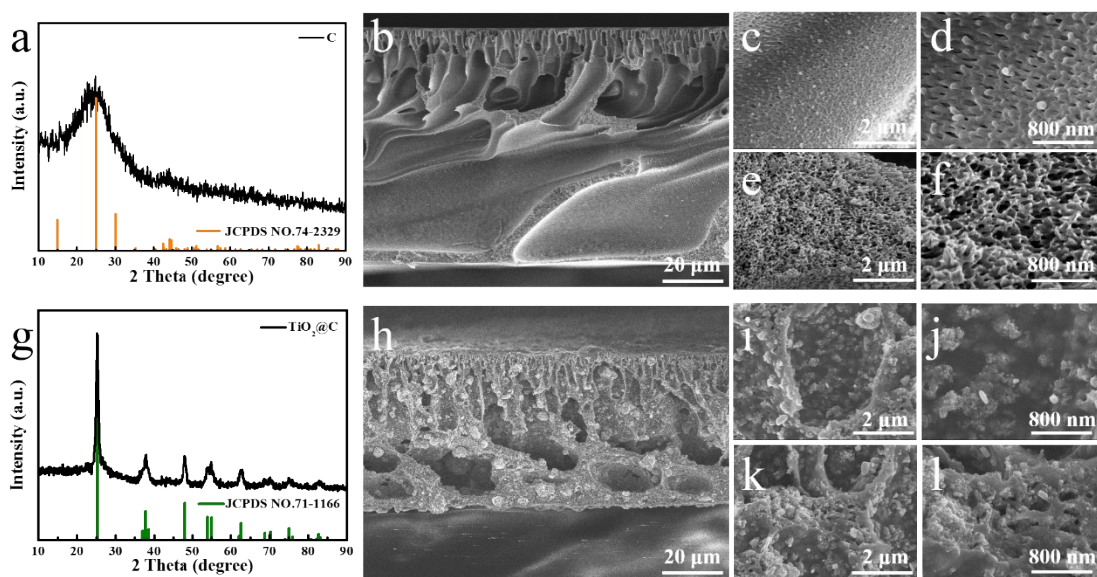


Figure S2 (a) XRD patterns of C membrane and corresponding PDF card; SEM images of (b) the cross section of C membrane, (c, d) the internal pore surface of C membrane, (e, f) the cross section of the pore wall of C membrane; (g) XRD patterns of $\text{TiO}_2@\text{C}$ membrane and corresponding PDF card; SEM images of (h) the cross section of $\text{TiO}_2@\text{C}$ membrane, (i, j) the internal pore surface of $\text{TiO}_2@\text{C}$ membrane, (k, l) the cross section of the pore wall of $\text{TiO}_2@\text{C}$ membrane.

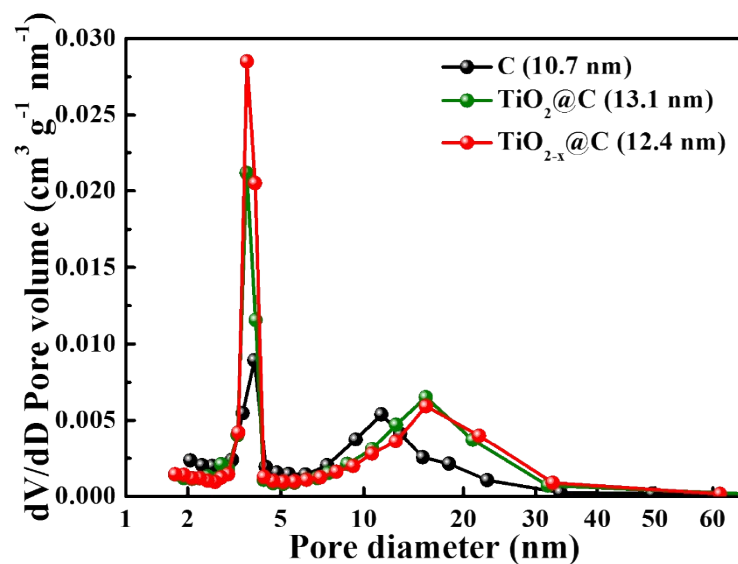


Figure S3 Pore size distribution of C membrane, $\text{TiO}_2@\text{C}$ membrane and $\text{TiO}_{2-x}@\text{C}$ membrane.

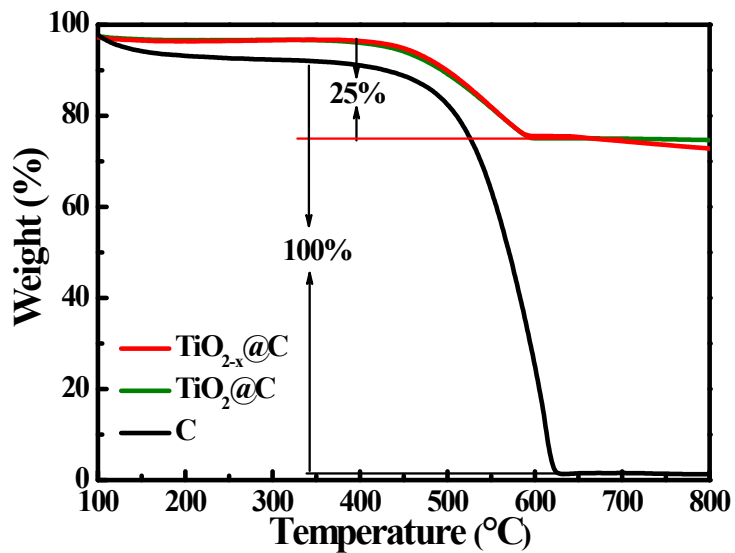


Figure S4 Thermogravimetric analysis of C, TiO_2 @C membrane and TiO_{2-x} @C membrane.

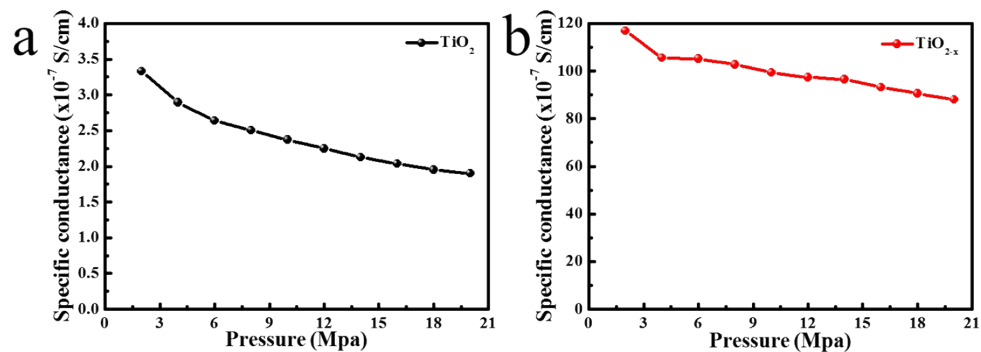


Figure S5 Specific conductance evaluations of (a) TiO_2 and (b) TiO_{2-x} .

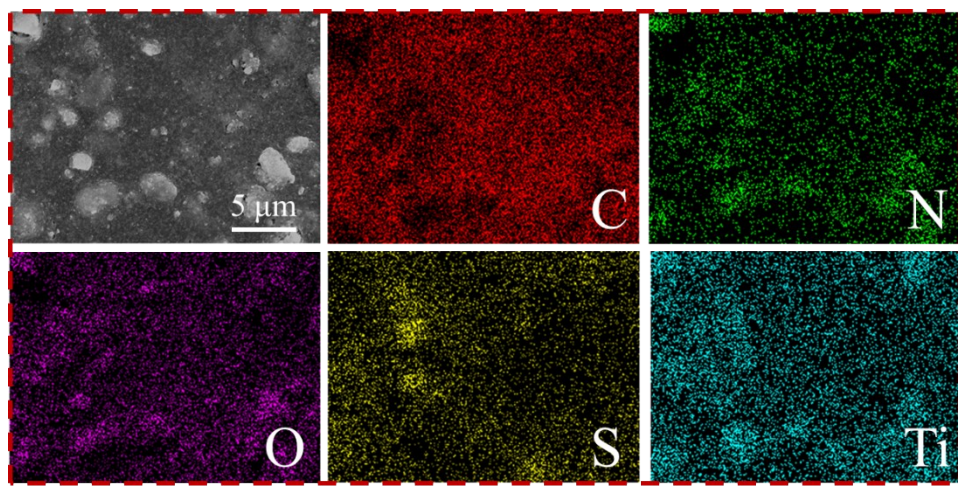


Figure S6 EDS mapping of the plane of $\text{TiO}_{2-x}@\text{C/S}$ membrane.

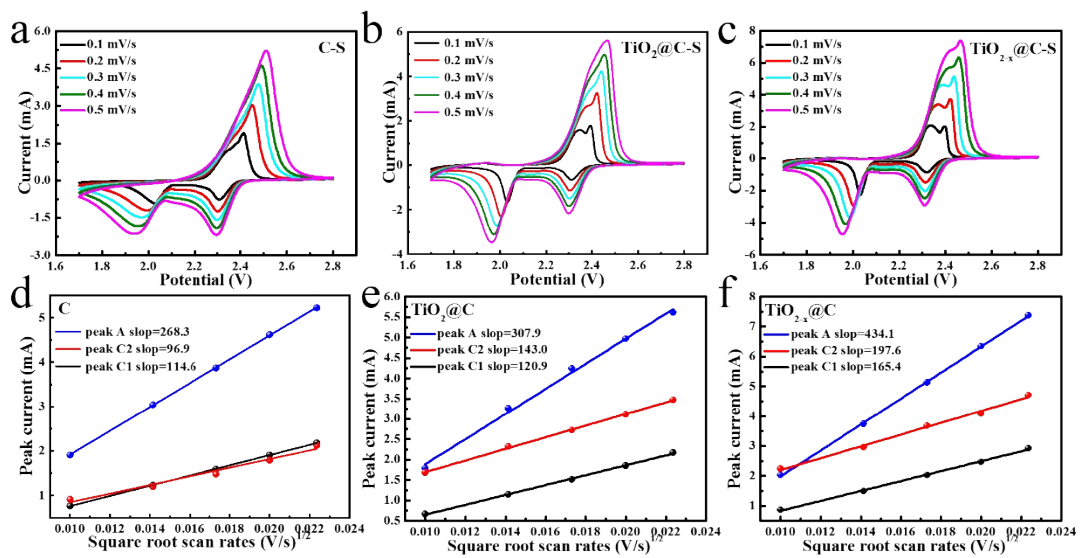


Figure S7 CV curves of different scanning rate of (a) C/S membrane electrode, (b) $\text{TiO}_2@\text{C/S}$ membrane electrode, (c) $\text{TiO}_{2-x}@\text{C/S}$ membrane electrode; Plots of peak CV current for (d) C/S membrane electrode, (e) $\text{TiO}_2@\text{C/S}$ membrane electrode, (f) $\text{TiO}_{2-x}@\text{C/S}$ membrane electrode.

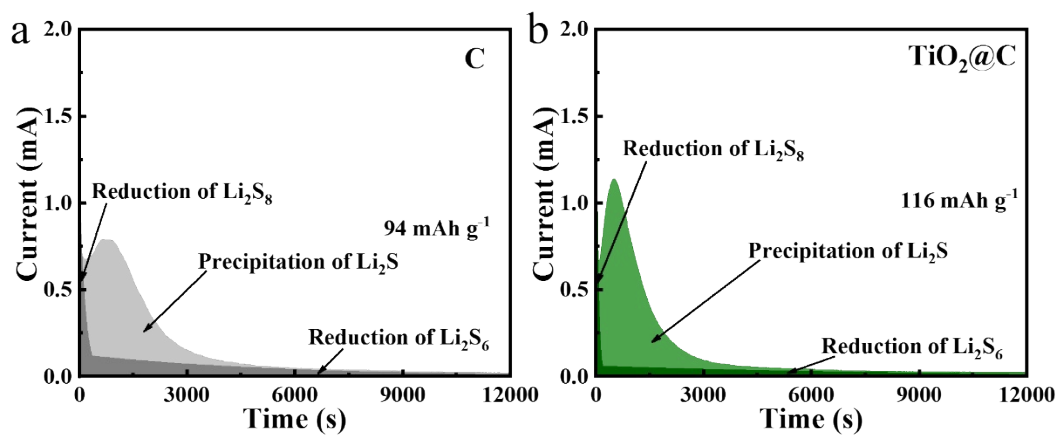


Figure S8 Potentiostatic discharge curve of Li₂S₈ solution at 2.05 V on (a) C membrane and (b) TiO₂@C membrane.

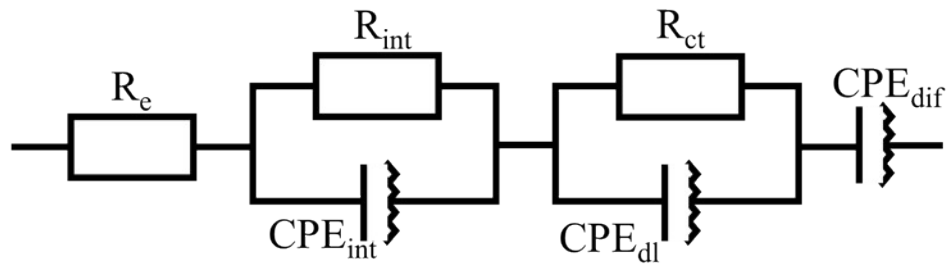


Figure S9 The equivalent circuit.

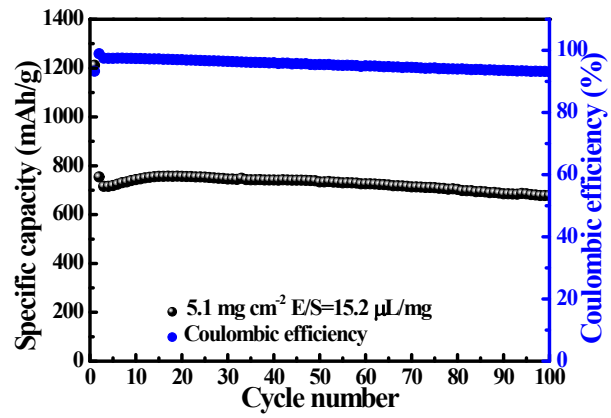


Figure S10 Cycling performance of the $\text{TiO}_{2-x}@\text{C}/\text{S}$ membrane electrode under different sulfur loading at 0.5 C.

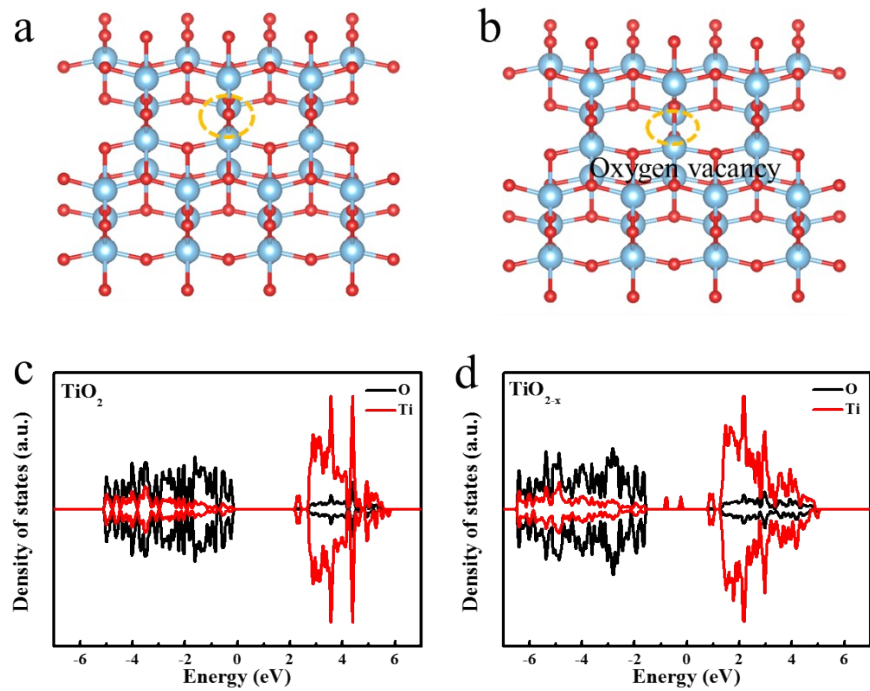


Figure S11 DFT-calculated structures of (a) TiO_2 and (b) TiO_{2-x} ; Density of states of (c) TiO_2 and (d) TiO_{2-x}

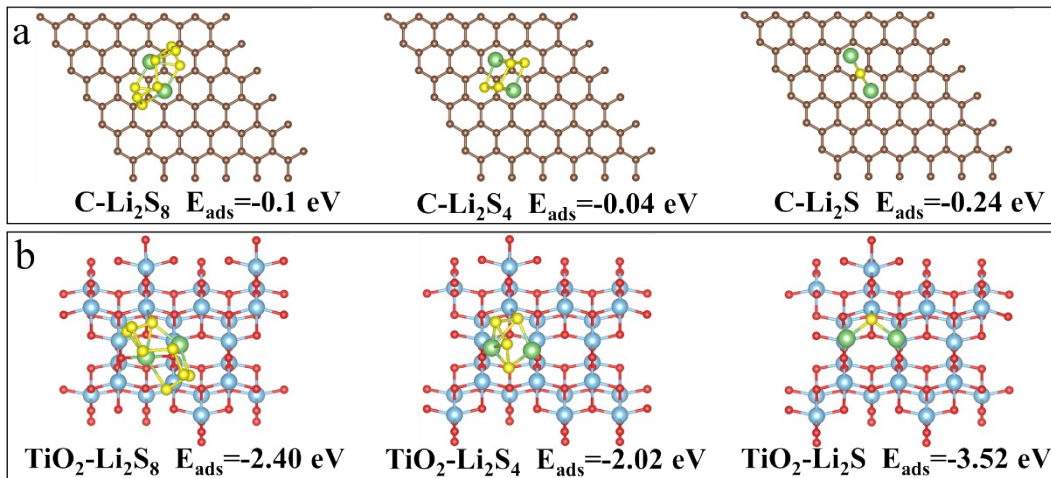


Figure S12 DFT-calculated structures and adsorption energies of Li_2S_8 , Li_2S_4 and Li_2S on the (a) C and (b) TiO_2 .

Table S1 Calculated slopes of fitting CV curves with different sweep rate.

Slop (mA/(V/s) $^{1/2}$)	C membrane	$\text{TiO}_2@\text{C}$ membrane	$\text{TiO}_{2-x}@\text{C}$ membrane
C1	114.6	120.9	165.4
C2	96.9	143.0	197.6
A	268.3	307.9	434.1

Table S2 Comparison of EIS fitting results for C/S, $\text{TiO}_2@\text{C/S}$ and $\text{TiO}_{2-x}@\text{C/S}$ cathodes.

Cathode materials	$R_e(\Omega)$	$R_{\text{int}}(\Omega)$	$R_{\text{ct}}(\Omega)$
C/S	3.3	21.1	211.7
$\text{TiO}_2@\text{C/S}$	2.21	15.3	123.8
$\text{TiO}_{2-x}@\text{C/S}$	4.8	5.2	79.9

Table S3 Electrochemical performance of Li-S batteries based on TiO₂.

Materials	Rate (C)	Cycle	Specific capacity (mAh g ⁻¹)	Ref.
TiO _{2-x} @C	0.5	100	877.9	This work
TiO _{2-x} @C	2	500	715.2	This work
“Room-like” TiO ₂ Array	0.5	150	770	8
TiO ₂ nanosheets/N-doped carbon	2	900	350.8	9
TiO ₂ @NiCo-LDH-PAN	1	200	699.3	10
TiO ₂ @GA	0.2	100	905	11
mesoporous carbon/TiO ₂	2	500	658	12
yolk-shell TiO ₂	2	400	511	13
PCS/TO ₂	0.5	170	427	14
titanium-deficient anatase TiO ₂	2	1000	488	15
TiO ₂ -Xene heterojunction framework	1	500	723.3	16
TiO ₂ nanotube/RGO	0.2	100	620.6	17

References

1. G. Kresse and J. Furthmüller, *Computational Materials Scienc*, 1996, **6**, 15-50.
2. G. Kresse and J. Furthmüller, *Physical Review B*, 1996, **54**, 11169-11186.
3. J. P. Perdew, K. Burke and M. Ernzerhof, *Physical Review Letters*, 1996, **77**, 3865-3868.
4. G. Kresse and D. Joubert, *Physical Review B*, 1999, **59**, 1758-1775.
5. P. E. Blöchl, *Physical Review B*, 1994, **50**, 17953-17979.
6. S. L. Dudarev, G. A. Botton, S. Y. Savrasov, C. J. Humphreys and A. P. Sutton, *Physical Review B*, 1998, **57**, 1505-1509.
7. S. Grimme, J. Antony, S. Ehrlich and H. Krieg, *The Journal of Chemical Physics*, 2010, **132**, 154104-154120.
8. J. Guo, S. Zhao, Y. Shen, G. Shao and F. Zhang, *ACS Sustainable Chemistry & Engineering*, 2020, **8**, 7609-7616.
9. N. Li, F. Chen, X. Chen, Z. Chen, Y. Qi, X. Li and X. Sun, *Journal of Materials Science & Technology*, 2020, **55**, 152-158.
10. F. Lan, H. Zhang, J. Fan, Q. Xu, H. Li and Y. Min, *ACS Applied Materials & Interfaces*, 2021, **13**, 2734-2744.

11. M. Wang, S. Tan, S. Kan, Y. Wu, S. Sang, K. Liu and H. Liu, *Journal of Energy Chemistry*, 2020, **49**, 316-322.
12. S. Liu, C. Li and D. Liu, *Journal of Alloys and Compounds*, 2021, **862**, 158381-158386.
13. Y. Yu, M. Yan, W.-D. Dong, L. Wu, Y.-W. Tian, Z. Deng, L.-H. Chen, T. Hasan, Y. Li, B.-L. Su, *Chemical Engineering Journal*, 2021, **417**, 129241-129250.
14. T. Zerrin, M. Kurban, M. M. Dickson, M. Ozkan and C. S. Ozkan, *ACS Applied Energy Materials*, 2020, **3**, 1515-1529.
15. J. Yang, L. Xu, S. Li and C. Peng, *Nanoscale*, 2020, **12**, 4645-4654.
16. R. Hou, S. Zhang, P. Zhang, Y. Zhang, X. Zhang, N. Li, Z. Shi and G. Shao, *Journal Materials Chemistry A*, 2020, **8**, 25255-25267.
17. Y. Gui, P. Chen, D. Liu, Y. Fan, J. Zhou, J. Zhao, H. Liu, X. Guo, W. Liu and Y. Cheng, *Journal of Alloys and Compounds*, 2022, **895**, 162495-162504.